Improved Finite-Difference Time-Domain Algorithm Based on Error Control for Lossy Materials

Theodoros T. Zygiridis and Theodoros D. Tsiboukis, *Senior Member, IEEE*

Abstract—This paper discusses the development of a reduced-error finite-difference time-domain algorithm, capable of handling conducting media in an efficient manner. Founded on a spatially extended stencil, the proposed scheme introduces a novel design procedure, whose basic idea is to enforce conditions of the continuous space to the discrete level. In this way, we derive reliable space–time models for 2-D Maxwell's equations, minimizing the inherent phase and amplitude deviations. A high degree of adaptivity is also accomplished, as the spectral reliability range can be adjusted according to problem-dependent needs. Consequently, an upgraded discretization strategy is provided, which exhibits the same computational complexity with the conventional scheme.

Index Terms—Finite-difference time-domain (FDTD) methods, high-order schemes, lossy media, optimized algorithms.

I. INTRODUCTION

DESPITE THE growing amount of available computational power and resources, the development of efficient numerical methods for electromagnetic (EM) wave phenomena remains a particularly active research topic. In this context, the foundation of high-order finite-difference time-domain (FDTD) techniques has been the subject of various publications (see, e.g., [1] and the references therein), providing attractive alternatives for Yee's classic second-order algorithm [2], [3]. In recent years, innovative formulations have been proposed for an emerging class of reliable FDTD approaches, which facilitate performance tuning and behavior optimization according to case-related requirements [4]–[12]. Such schemes can accomplish further accuracy enhancement for a given computational stencil (i.e., without affecting the entailed computational cost), by avoiding the shortcomings of the standard—based on Taylor series—approximate operators.

Unfortunately, most of the aforementioned approaches are suited for configurations involving lossless materials only, a feature that hinders their generalized application. Electrically conducting spaces are almost always overlooked, probably due to the fact that theoretical error estimates become troublesome (or even impossible) under such circumstances. To some degree, these difficulties can be associated with the simultaneous presence of phase and amplitude errors in discretized lossy media [13], in contrast to pure phase artifacts of nonconducting areas. Yet, it is a common belief that optimized FDTD dicretizations may never be extensively utilized unless they are capable of dealing with a wide variety of EM features.

This paper is devoted to a new variant of the FDTD method, which aims at the reliable modeling of wave interactions in lossy spaces, considering 2-D geometries. The proposed algorithm is structurally similar to the $(2, 4)$ scheme [14], as it combines the second-order leapfrog integration with four-point spatial expressions. While simple to implement, this methodology accomplishes low error levels by altering the form of the approximate space–time operators, without affecting the size of the adopted computational stencil. Both phase and amplitude errors are mitigated to a satisfactory degree, thanks to a novel design procedure developed for the derivation of the technique's constituent elements. In essence, physical conditions that govern wave behavior in continuous lossy areas are required to hold in the discrete domain as well, thus guaranteeing the preservation of fundamental EM properties. By further controlling the bandwidth of the scheme's spectral reliability, a high level of flexibility is attained, which we deem a necessary attribute for the successful handling of problems with diverse nature. In the remainder of this paper, the foundation of the new approach is analytically presented, and its properties are analyzed via various theoretical studies and numerical simulations.

II. METHODOLOGY

We will be studying the 2-D case of TE_z waves (E_x, E_y, and H_z components); the treatment of TM_z waveforms can be conducted in a similar manner.

Let us consider a homogeneous medium with electric permittivity ϵ, magnetic permeability μ, and electric conductivity σ. For the TE_z case, Maxwell's equations reduce to the system

$$\begin{bmatrix} \epsilon \dfrac{\partial}{\partial t} + \sigma & 0 & -\dfrac{\partial}{\partial y} \\ 0 & \epsilon \dfrac{\partial}{\partial t} + \sigma & \dfrac{\partial}{\partial x} \\ -\dfrac{\partial}{\partial y} & \dfrac{\partial}{\partial x} & \mu \dfrac{\partial}{\partial t} \end{bmatrix} \begin{bmatrix} E_x \\ E_y \\ H_z \end{bmatrix} = [0] \qquad (1)$$

if sources are absent. This paper's methodology attempts the reliable transfer of certain physical conditions [extracted from (1)] from the continuous to the discrete state. In other words, numerical operators are designed so that the aforementioned requirement is fulfilled. Apparently, electric and magnetic fields do not satisfy identical conditions, as the third equation is structurally different from the first two. Therefore, we opt to treat the corresponding approximations separately.

Assuming plane-wave propagation along $\widehat{\mathbf{n}} = \cos\phi\widehat{\mathbf{x}} + \sin\phi\widehat{\mathbf{y}}$ (Fig. 1), the electric-field intensity can be written as

$$\mathbf{E} = E_0 e^{j\omega t - \boldsymbol{\gamma}\cdot\mathbf{r}} \left(-\sin\phi\widehat{\mathbf{x}} + \cos\phi\widehat{\mathbf{y}}\right) \qquad (2)$$
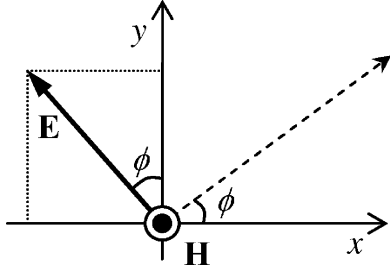
Fig. 1. 2-D configuration of a TE_z wave, propagating at angle ϕ.

where $\boldsymbol{\gamma} = \gamma \hat{\mathbf{n}}$ denotes the complex propagation constant ($\gamma = \sqrt{\jmath\omega\mu(\sigma + \jmath\omega\epsilon)} = \alpha + \jmath\beta$), and E_0 is a complex magnitude. For the magnetic-field intensity, we have

$$\mathbf{H} = \frac{E_0}{\eta} e^{\jmath\omega t - \boldsymbol{\gamma}\cdot\mathbf{r}} \hat{\mathbf{z}} \tag{3}$$

with $\eta = \jmath\omega\mu\gamma^{-1}$ being the medium's intrinsic impedance. Functions (2) and (3) comprise a solution set of (1).

We are considering an FDTD realization that utilizes the common second-order leapfrog integrator and generalized definitions of the spatial operators. For magnetic-field components, spatial derivatives are approximated by

$$\left.\frac{\widetilde{\partial H_z}}{\partial u}\right|_i = \frac{1}{\Delta u} \sum_{m=1}^{2} C_m^u \left(H_z|_{i+(2m-1)/2} - H_z|_{i-(2m-1)/2} \right) \tag{4}$$

for $u \in \{x, y\}$. Moreover, a weighted average of successive electric-field samples is selected for current-density terms

$$\langle E_u \rangle|^n = \frac{A^u}{2} \left(E_u|^{n+1/2} + E_u|^{n-1/2} \right). \tag{5}$$

By substituting the exact solutions (2) and (3) in the second equation of (1), and replacing the continuous operators with the approximate expressions (4) and (5), we are led to

$$\eta \left[\epsilon \mathcal{T}(\omega) + \sigma \mathcal{S}^y(\omega) \right] \cos\phi + \mathcal{X}^{\mathrm{m}}(\gamma) = 0 \tag{6}$$

where

$$\mathcal{X}^{\mathrm{m}}(\gamma) = -\frac{2}{\Delta x} \sum_{m=1}^{2} C_m^x \sinh\left[U_m(x, \gamma) \right] \tag{7}$$

$$\mathcal{T}(\omega) = \frac{2\jmath}{\Delta t} \sin\left(\frac{\omega \Delta t}{2} \right) \tag{8}$$

$$\mathcal{S}^u(\omega) = A^u \cos\left(\frac{\omega \Delta t}{2} \right) \tag{9}$$

$$U_m(a, b) = \frac{(2m-1) b_a \Delta a}{2} \tag{10}$$

and $a \in \{x, y\}$, $b \in \{\alpha, \beta, \gamma\}$. If the intrinsic impedance is analyzed as $\eta = \eta_1 + \jmath\eta_2$ ($\eta_1, \eta_2 \in \mathbb{R}$), then (6) becomes

$$\sum_{n=1}^{2} \left[\jmath^{n-1} \left(\sum_{m=1}^{2} \kappa_{nm} C_m^x + \zeta_n A^y + \lambda_n \right) \right] = 0 \tag{11}$$

where

$$\kappa_{1m} = -\frac{2}{\Delta x} \sinh\left[U_m(x, \alpha) \right] \cos\left[U_m(x, \beta) \right] \tag{12}$$

$$\kappa_{2m} = -\frac{2}{\Delta x} \cosh\left[U_m(x, \alpha) \right] \sin\left[U_m(x, \beta) \right] \tag{13}$$

$$\zeta_n = \sigma\eta_n \cos\left(\frac{\omega \Delta t}{2} \right) \cos\phi \tag{14}$$

$$\lambda_n = (-1)^n \frac{2}{\Delta t} \eta_{3-n} \epsilon \sin\left(\frac{\omega \Delta t}{2} \right) \cos\phi. \tag{15}$$

Notice that quantities (12)–(15) are real valued. Evidently, (11) still applies if the magnitude of its left-hand side vanishes as follows:

$$e(\omega, \phi) = \sum_{n=1}^{2} \left[\left(\sum_{m=1}^{2} \kappa_{nm} C_n^x + \zeta_n A + \lambda_n \right) \right]^2 = 0. \tag{16}$$

Since the above equation has been derived assuming an exact solution of Maxwell's equations, approximations (4) and (5) that comply with (16) will be exact as well. Unfortunately, (16) generally represents a strict requirement that cannot be satisfied by an FDTD method for all propagation angles and wavelengths due to the finite differences' inherent anisotropy, dispersion, and loss. Exact solutions for the unknowns C_1^x, C_2^x, and A^y could probably be determined for a selected pair (ω_0, ϕ_0) degrading, however, the scheme's global character. Instead, we attempt to make the frequency- and angle-dependent function defined in (16) as close to zero as possible in an average sense. We expect that sufficiently small values of $e(\omega, \phi)$ should guarantee accurate simulations since they would imply a good approximation of the continuous state. Given that, in most cases, algorithmic reliability is required: 1) within a specific frequency band ($\omega_1 < \omega < \omega_2$) and 2) for all directions ($0 < \phi < 2\pi$), we define the total error according to

$$\mathcal{E} = \int_0^{2\pi} \int_{\omega_1}^{\omega_2} e(\omega, \phi) \, d\omega d\phi. \tag{17}$$

In case of time–harmonic or narrowband situations, it suffices to select a specific value for ω and perform single integration over $\phi \in \begin{bmatrix} 0 & 2\pi \end{bmatrix}$ in (17).

The minimization of $\mathcal{E}$ calls for the vanishing of $\nabla\mathcal{E}$ with respect to C_1^x, C_2^x, and A^y, leading to a 3×3 system

$$\begin{bmatrix} a_{11} & a_{12} & a_{13} \\ a_{21} & a_{22} & a_{23} \\ a_{31} & a_{32} & a_{33} \end{bmatrix} \begin{bmatrix} C_1^x \\ C_2^x \\ A^y \end{bmatrix} = \begin{bmatrix} b_1 \\ b_2 \\ b_3 \end{bmatrix}. \tag{18}$$

If we introduce

$$I(f) = \int_0^{2\pi} \int_{\omega_1}^{\omega_2} f \, d\omega d\phi \tag{19}$$

then, for $n = 1, 2$, it is $a_{nn} = I\left(\kappa_{1n}^2 + \kappa_{2n}^2 \right)$, $a_{33} = I\left(\zeta_1^2 + \zeta_2^2 \right)$, $a_{12} = a_{21} = I\left(\kappa_{11}\kappa_{12} + \kappa_{21}\kappa_{22} \right)$, $a_{n3} = a_{3n} = I\left(\kappa_{1n}\zeta_1 + \kappa_{2n}\zeta_2 \right)$, $b_n = -I\left(\lambda_1\kappa_{1n} + \lambda_2\kappa_{2n} \right)$, and $b_3 = -I\left(\lambda_1\zeta_1 + \lambda_2\zeta_2 \right)$. Consequently, the solution of (18) determines the discretization of the second equation of (1). Regarding the first equation, the same procedure can be applied,

leading to a similar system for C_1^y, C_2^y, and A^x. Due to the complicated form of (12)–(15), all integrations are performed numerically.

In order to formulate difference approximations for the spatial operators applied to electric-field components, we consider the third equation of (1). Derivatives are now expressed as

$$\left.\frac{\widetilde{\partial}E_v}{\partial u}\right|_i = \frac{1}{\Delta u}\sum_{m=1}^{2} D_m^u \left(E_v|_{i+(2m-1)/2} - E_v|_{i-(2m-1)/2} \right) \tag{20}$$

where $(u,v) \in \{(x,y),(y,x)\}$. By following the procedure described previously, we obtain

$$\eta^{-1}\mu\mathcal{T}(\omega) + \mathcal{Y}^e(\gamma)\sin\phi + \mathcal{X}^e(\gamma)\cos\phi = 0 \tag{21}$$

where

$$\mathcal{X}^e(\gamma) = -\frac{2}{\Delta x}\sum_{m=1}^{2} D_m^x \sinh\left[U_m(x,\gamma)\right] \tag{22}$$

$$\mathcal{Y}^e(\gamma) = -\frac{2}{\Delta y}\sum_{m=1}^{2} D_m^y \sinh\left[U_m(y,\gamma)\right]. \tag{23}$$

Again, (21) represents the outcome from discretizing a physical condition. This can be satisfied in a mean-value sense if the corresponding unknowns are determined from the solution of specific equations

$$\begin{bmatrix} a_{11} & a_{12} & a_{13} & a_{14} \\ a_{21} & a_{22} & a_{23} & a_{24} \\ a_{31} & a_{32} & a_{33} & a_{34} \\ a_{41} & a_{42} & a_{43} & a_{44} \end{bmatrix}\begin{bmatrix} D_1^x \\ D_2^x \\ D_1^y \\ D_2^y \end{bmatrix} = \begin{bmatrix} b_1 \\ b_2 \\ b_3 \\ b_4 \end{bmatrix}. \tag{24}$$

By defining

$$\kappa_{1m} = -\frac{2}{\Delta x}\sinh\left[U_m(x,\alpha)\right]\cos\left[U_m(x,\beta)\right]\cos\phi \tag{25}$$

$$\kappa_{2m} = -\frac{2}{\Delta x}\cosh\left[U_m(x,\alpha)\right]\sin\left[U_m(x,\beta)\right]\cos\phi \tag{26}$$

$$\nu_{1m} = -\frac{2}{\Delta y}\sinh\left[U_m(y,\alpha)\right]\cos\left[U_m(y,\beta)\right]\sin\phi \tag{27}$$

$$\nu_{2m} = -\frac{2}{\Delta y}\cosh\left[U_m(y,\alpha)\right]\sin\left[U_m(y,\beta)\right]\sin\phi \tag{28}$$

$$\lambda_n = \frac{2\mu\eta_{3-n}}{(\eta_1^2 - \eta_2^2)\Delta t}\sin\left(\frac{\omega\Delta t}{2}\right) \tag{29}$$

then it is $a_{nn} = I\left(\kappa_{1n}^2 + \kappa_{2n}^2\right)$ for $n = 1, 2$, $a_{nn} = I\left(\nu_{1(n-2)}^2 + \nu_{2(n-2)}^2\right)$ for $n = 3, 4$, $a_{12} = a_{21} = I(\kappa_{11}\kappa_{12} + \kappa_{21}\kappa_{22})$, $a_{13} = a_{31} = I(\kappa_{11}\nu_{11} + \kappa_{21}\nu_{21})$, $a_{14} = a_{41} = I(\kappa_{11}\nu_{12} + \kappa_{21}\nu_{22})$, $a_{23} = a_{32} = I(\kappa_{12}\nu_{11} + \kappa_{22}\nu_{21})$, $a_{24} = a_{42} = I(\kappa_{12}\nu_{12} + \kappa_{22}\nu_{22})$, $a_{34} = a_{43} = I(\nu_{11}\nu_{12} + \nu_{21}\nu_{22})$, $b_n = -I(\lambda_1\kappa_{1n} + \lambda_2\kappa_{2n})$ for $n = 1, 2$, and $b_n = -I\left(\lambda_1\nu_{1(n-2)} + \lambda_2\nu_{2(n-2)}\right)$ for $n = 3, 4$.

III. PERFORMANCE

For the described numerical technique, the characteristic dispersion relation can be obtained by substituting appropriate

Fourier modes in the discretized version of (1), producing

$$\mathcal{X}^e(\widetilde{\gamma})\,\mathcal{X}^m(\widetilde{\gamma}) + \mathcal{Y}^e(\widetilde{\gamma})\,\mathcal{Y}^m(\widetilde{\gamma})\frac{\epsilon\mathcal{T} + \sigma\mathcal{S}_y}{\epsilon\mathcal{T} + \sigma\mathcal{S}_x} = \mu\mathcal{T}(\epsilon\mathcal{T} + \sigma\mathcal{S}_y) \tag{30}$$

with $\widetilde{\gamma}$ being the numerical propagation constant. Recall that the latter is a complex quantity and, therefore, the approximate scheme induces both phase and amplitude errors. Furthermore, a stability analysis [3], [7] reveals that bounded solutions are guaranteed if temporal sampling complies with

$$\frac{\Delta t}{\sqrt{\mu\epsilon}} \leq \left\{\sum_{u\in\{x,y\}}\left[\frac{(C_1^u - C_2^u)(D_1^u - D_2^u)}{\Delta u}\right]^2\right\}^{-1/2}. \tag{31}$$

In order to facilitate accuracy studies, the discretization error at an angular frequency ω is estimated via

$$e_{2\text{-D}}(\omega) = \frac{1}{2\pi}\int_0^{2\pi}\left|1 - \frac{\widetilde{\gamma}(\omega,\phi)}{\gamma(\omega)}\right|d\phi. \tag{32}$$

Apparently, this definition takes into account all possible directions of propagation equally, implicitly incorporating every error-producing mechanism. In fact, $e_{2\text{-D}}$ represents a measure of the average error pertinent to the propagation constant, and is expected to behave more reliably compared to other common choices such as the maximum absolute error (which actually overlooks the anisotropic behavior).

Consider now a lossy medium with $\epsilon_r = 3$, $\sigma = 0.01$ S/m, with our interest focused around the central frequency $f_0 = 1$ GHz ($\tan\delta_0 = \sigma/\omega_0\epsilon \simeq 0.06$). The capabilities of the new scheme are revealed by calculating $e_{2\text{-D}}(\omega)$ for various design frequencies, which designate different bandwidths

$$\text{BW} = \frac{f_2 - f_1}{f_0}100\%. \tag{33}$$

In (33), $f_1 = \omega_1/2\pi$ and $f_2 = \omega_2/2\pi$ denote the lower and upper optimization points, respectively. The selected grid resolution corresponds to 20 cells per wavelength at f_0, and the time step is set to $0.85\Delta/\sqrt{2}c_0$ (Δ is the spatial step). Fig. 2 plots $e_{2\text{-D}}$ as a function of frequency, when BW is equal to 30%, 60%, or 90%. The case of single-frequency optimization at f_0 is also shown. As seen, the error curves are adjusted according to the requirements prescribed through the optimization process. High-frequency errors also become comparable to—or weaker than—those emerging in the lower bands, a quality not exhibited by conventional difference operators. Another interesting observation is that, according to numerical evidence (see, for instance, Table I), $e_{2\text{-D}}$ exhibits a fourth-order convergence rate at f_0 when single-frequency tuning is performed. Thanks to the combined treatment of space–time errors, inaccuracies are minimized in a mean-value fashion so that algorithmic performance is essentially controlled by anisotropic features only. This attribute also renders our approach fundamentally different from the standard $(2,4)$ scheme since the latter calls for undesirably small time steps in order to attain such a spectral response.
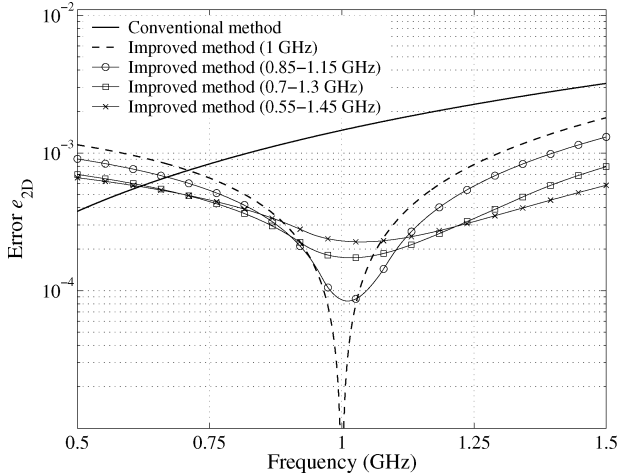
Fig. 2. Error $e_{\text{2-D}}$ versus frequency for different bandwidth choices.

Fig. 3. Error e_{I} versus cells size for different bandwidths and materials.

TABLE I
ERROR $e_{\text{2-D}}$ FOR VARIOUS DISCRETIZATIONS AND MAXIMUM TIME
STEPS AT 1 GHz WHEN $\epsilon_r = 3$ AND $\sigma = 0.02$ S/m
(THE IMPROVED SCHEME IS OPTIMIZED AT 1 GHz)

Spatial step	Standard (2,4) method		Improved (2,4) method	
	e_{2D} @ 1 GHz	Rate	e_{2D} @ 1 GHz	Rate
$\lambda/5$	1.78e − 2		4.38e − 4	
$\lambda/10$	5.60e − 3	1.86	2.53e − 5	4.03
$\lambda/20$	1.48e − 3		1.56e − 6	
$\lambda/40$	3.76e − 4		1.01e − 7	

Next, the overall error produced within more extensive parts of the spectrum is calculated according to the formula

$$e_{\text{I}} = \frac{1}{\omega_2 - \omega_1} \int_{\omega_1}^{\omega_2} e_{\text{2-D}}(\omega)\,d\omega. \qquad (34)$$

The considered cases refer to two different bandwidths (30% and 60%), as well as two conductivity values (0.01 and 0.3 S/m) for $f_0 = 1$ GHz and a medium with $\epsilon_r = 3$. Note that the integral's limits in (34) are selected to coincide with the design points. The e_{I} estimates, plotted in Fig. 3 versus grid density, are indicative of the modified $(2,4)$ scheme's performance. Evidently, the algorithm demonstrates—as probably expected—second-order behavior in wideband simulations, providing at the same time significant error mitigation, for varying bandwidths and media parameters.

Note that no limitations regarding the values of the background permittivities or conductivities have been introduced, implying that the proposed method can handle a wide range of materials. Nevertheless, one should keep in mind that optimized schemes are probably not necessary for the discretization of highly lossy structures. In such cases, the propagating nature of EM fields is diminished due to severe attenuation and, consequently, excessive numerical errors are less likely to emerge or spread throughout the computational domain.

IV. NUMERICAL RESULTS

In the first numerical demonstration, we examine the single-mode support by a lossy parallel-plate waveguide. The structure's size is 57.15 cm × 2.286 cm, and the electric characteristics of the background medium are described by $\epsilon_r = 2.5$ and $\sigma = 0.01$ S/m. In essence, propagation of the second TM mode is simulated, which is excited at 10 GHz by enforcing the exact field distribution at the configuration's ports throughout the time-stepping process. Initial values are assigned according to the exact solution as well, while the perfectly conducting boundaries are treated via proper symmetric or antisymmetric conditions with the aid of additional image nodes. To compare the performances of Yee's method, the standard $(2,4)$ and the improved $(2,4)$ techniques, simulations are carried out with lattices comprising 250 m × 10 m cells, $m = 1, 2, 4, 8$ for $4000m$ time steps. For $m = 1$ we have $C_1^u = 1.12527112$, $C_2^u = 0.04479331$, $D_1^u = 1.12725418$, $D_2^u = -0.04555975$, and $A^u = 1.01713586$. The maximum $L_2(t)$ error,
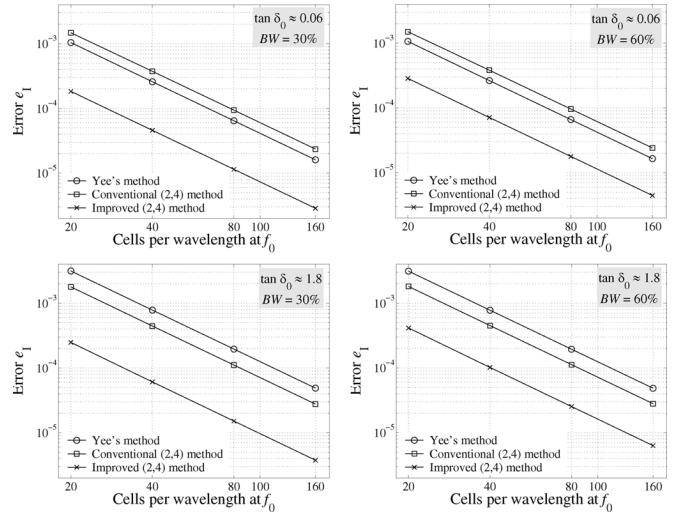
$$L_2(t) = \sqrt{\frac{\sum_{i,j}\left(H_z|_{i+1/2,j+1/2}^{n+1/2} - H_z^{\text{exact}}|_{i+1/2,j+1/2}^{n+1/2}\right)^2}{i_{\max}j_{\max}}} \qquad (35)$$

is given in Fig. 4 as a function of computational time (simulations are performed on a workstation with a Pentium 4–3.8-GHz processor). In this time–harmonic problem, the improved scheme accomplishes fourth-order convergence, which is in contrast to the second-order rate of the other two approaches. Clearly, phase and amplitude errors are efficiently mitigated, avoiding at the same time any extra computational cost. Similar conclusions can be drawn from Fig. 5, which exhibits the error versus the cell size for a larger conductivity ($\sigma = 0.05$ S/m). The slopes of the matching lines, derived through a least squares fitting, verify the aforementioned conclusions.

Next, the wideband capabilities of the proposed scheme are tested in the case of multimodal propagation in a 2-D waveguide (22.86 cm × 2.286 cm size with $\epsilon_r = 2.5$, $\sigma = 0.01$ S/m). The simulated EM field is the superposition of the first three TM modes, excited at 8, 11, and 14 GHz, respectively. Boundary and initial values are determined according to the procedure of the previous example. The computational domain is discretized by $180m × 18m$ cell lattices, $m = 1, 2, 4, 8$, and the duration
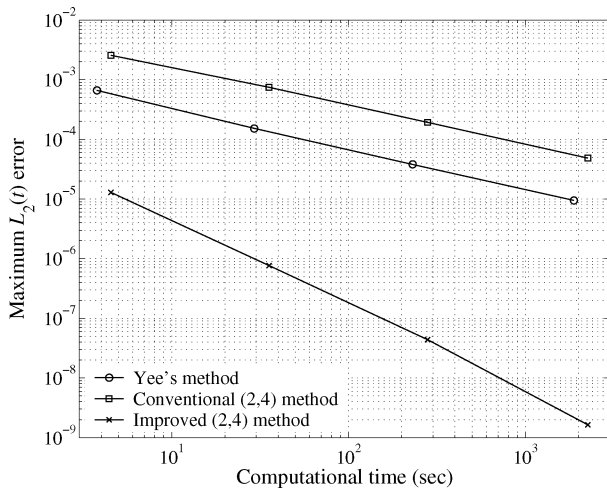
Fig. 4. Maximum $L_2(t)$ error versus required computational time in the single-mode waveguiding problem when $\sigma = 0.01$ S/m.
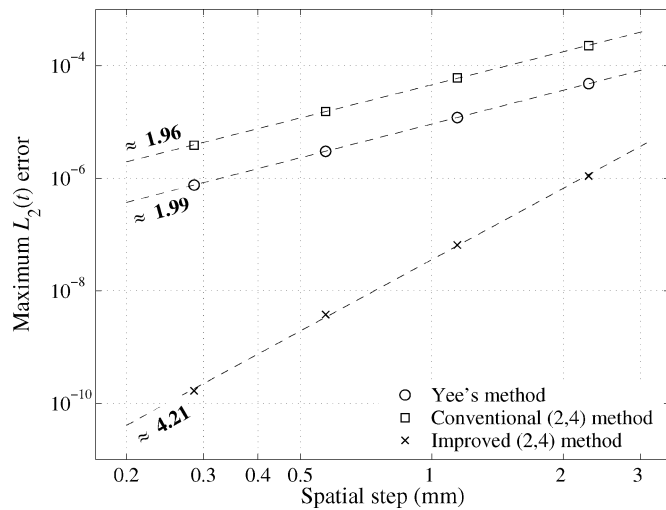

Fig. 6. Snapshot of the magnetic-field intensity along the waveguide under multimodal excitation.

Fig. 5. Maximum $L_2(t)$ error versus cell size in the single-mode waveguiding problem when $\sigma = 0.05$ S/m.

Fig. 7. Maximum $L_2(t)$ error versus the cell size in the 2-D waveguide simulation under multimodal excitation.

of each simulation is $4000m$ time steps. A snapshot of the calculated magnetic-field intensity is shown in Fig. 6 at the last time step, when $m = 1$. It can be seen that the accumulated error of the standard $(2,4)$ method induces unacceptable deviations, unlike the more valid results of the improved scheme. The dependence of the maximum $L_2(t)$ values on the size of the spatial steps is also depicted in Fig. 7, where improvement by an average factor of 7.7 is verified.

The following test is concerned with the resonant frequencies of a partially lossy rectangular cavity. In particular, a 10 mm $\times$ 6 mm cavity is modeled, which encloses a 4 mm $\times$ 2 mm lossy slab, located at its center ($\epsilon_r = 2$, $\sigma = 0.01$ S/m). To excite all modes, a Gaussian pulse is introduced at various points, and the emerging waveforms are recorded at preselected positions. Spatial steps of 0.5 mm are chosen, and the duration of the simulation is 32 768 time steps. The results obtained from a $10\times$ denser grid serve as reference. For the parts of the cavity not occupied by lossy material, optimized operators are derived by adjusting the design procedure of Section II to lossless free space ($\epsilon_r = 1$,
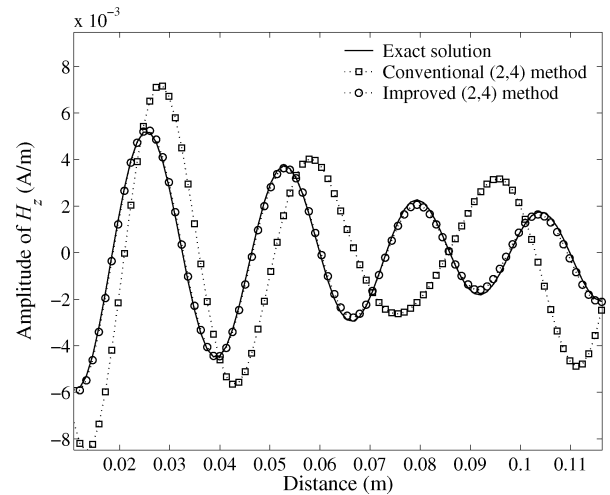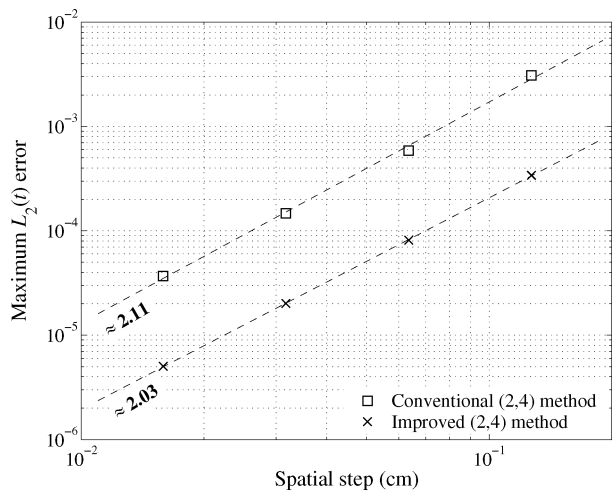
$\sigma = 0$). Arithmetic averaging of the constitutive parameters is applied on the material interfaces; therefore, some additional artifacts are expected due to this simplified treatment. The absolute error regarding the resonant frequencies of the first 14 modes is plotted in Fig. 8 (the band of interest extends from 14.9 to 74.8 GHz). As shown, errors are significantly reduced in the case of the optimized technique, a fact quite evident at higher frequencies. Apparently, a more sophisticated handling of the media discontinuities (e.g., [15] and [16]) should lead to even better accuracy.

We finally present a result regarding plane-wave scattering from an electrically large conducting rectangular target. The size of the latter is 2.75 m $\times$ 30 cm with $\epsilon_r = 2.2$ and $\sigma = 0.06$ S/m. The incident waveform is a horizontally propagating modulated Gaussian pulse with its central frequency located at 7 GHz. The size of the computational domain is 616×126 cells, including an eight-layer perfectly matched surrounding absorber [17]. The design frequencies are selected 4.5 and 9.5 GHz, according to the spectral content of the incident field. The discretization scheme within
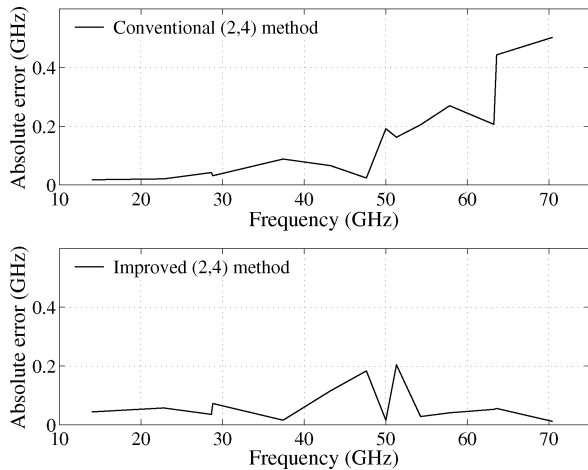
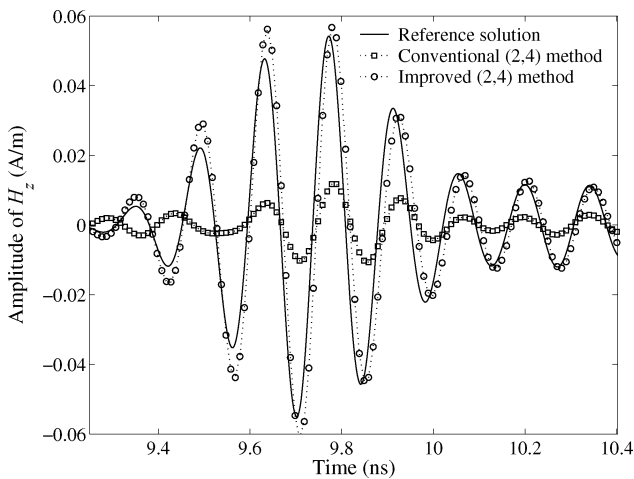Fig. 8. Error in determining the resonant frequencies of a lossy cavity.

Fig. 9. Time evolution of the magnetic field in the wave-scattering problem.

the scatterer introduces the parameters $C_1^u = 1.13309786$, $C_2^u = -0.04750884$, $A^u = 1.0115051$, $D_1^u = 1.13152537$, and $D_2^u = -0.04672861$. Fig. 9 depicts the calculated waveform at a point close to the right side of the scatterer (a reference solution has been obtained with a $5\times$ denser lattice). As noticed, the improved scheme avoids severe distortions and reproduces EM fields reliably, even with coarse discretizations.

V. Conclusion

A modified $(2, 4)$ FDTD scheme, capable of reducing phase and amplitude inaccuracies in lossy media, has been proposed in this paper. Through a novel design procedure, we have determined optimized approximations by requiring the validity of specific physical conditions on the discrete level, thus avoiding the drawbacks of conventional operators. The algorithm also exhibits adaptive capabilities, as it allows explicit control of its bandwidth (i.e., its spectral reliability range) according to case-related requirements. Without altering the entailed computational burden, the new scheme outperforms the standard

one, as proven by theoretical and experimental evidence. The pertinent ideas could be potentially applied to different stencils as well, investigating the possibility of even better wideband responses. The generalization of the presented approach to 3-D spaces will also enable its integration with other optimized methods, originally derived for lossless media.

References

[1] E. Turkel, "High-order methods," in *Advances in Computational Electromagnetics: The Finite-Difference Time-Domain Method*, A. Taflove, Ed. Norwood, MA: Artech House, 1998, ch. 2, pp. 63–110.

[2] K. S. Yee, "Numerical solution of initial boundary value problems involving Maxwell's equations in isotropic media," *IEEE Trans. Antennas Propag.*, vol. AP-14, no. 5, pp. 302–307, May 1966.

[3] A. Taflove and S. C. Hagness, *Computational Electrodynamics: The Finite-Difference Time-Domain Method*. Norwood, MA: Artech House, 2005.

[4] M. F. Hadi and M. Piket-May, "A modified FDTD (2, 4) scheme for modeling electrically large structures with high-phase accuracy," *IEEE Trans. Antennas Propag.*, vol. 45, no. 2, pp. 254–264, Feb. 1997.

[5] J. B. Cole, "A high-accuracy realization of the Yee algorithm using nonstandard finite differences," *IEEE Trans. Microw. Theory Tech.*, vol. 45, no. 6, pp. 991–996, Jun. 1997.

[6] E. A. Forgy and W. C. Chew, "A time-domain method with isotropic dispersion and increased stability on an overlapped lattice," *IEEE Trans. Antennas Propag.*, vol. 50, no. 7, pp. 983–996, Jul. 2002.

[7] S. Wang and F. L. Teixeira, "Dispersion-relation-preserving FDTD algorithms for large-scale three-dimensional problems," *IEEE Trans. Antennas Propag.*, vol. 51, no. 8, pp. 1818–1828, Aug. 2003.

[8] J. B. Cole, "High-accuracy FDTD solution of the absorbing wave equation, and conducting Maxwell's equations based on a nonstandard finite-difference model," *IEEE Trans. Antennas Propag.*, vol. 52, no. 3, pp. 725–729, Mar. 2004.

[9] G. Sun and C. W. Trueman, "Optimized finite-difference time-domain methods based on the $(2, 4)$ stencil," *IEEE Trans. Microw. Theory Tech.*, vol. 53, no. 3, pp. 832–842, Mar. 2005.

[10] B. Yang and C. A. Balanis, "An isotropy-improved nonstandard finite-difference time-domain method," *IEEE Trans. Antennas Propag.*, vol. 54, no. 7, pp. 1935–1942, Jul. 2007.

[11] B. Finkelstein and R. Kastner, "Finite difference time domain dispersion reduction schemes," *J. Comput. Phys.*, vol. 221, no. 1, pp. 422–438, 2007.

[12] T. T. Zygiridis and T. D. Tsiboukis, "Optimized three-dimensional FDTD discretizations of Maxwell's equations on Cartesian grids," *J. Comput. Phys.*, vol. 226, no. 2, pp. 2372–2388, Oct. 2007.

[13] G. Sun and C. W. Trueman, "Numerical dispersion and numerical loss in explicit finite-difference time-domain methods in lossy media," *IEEE Trans. Antennas Propag.*, vol. 53, no. 11, pp. 3684–3690, Nov. 2005.

[14] J. Fang, "Time domain computation for Maxwell's equations," Ph.D. dissertation, Dept. Elect. Eng. Comput. Sci., Univ. California at Berkeley, Berkeley, CA, 1989.

[15] A. Yefet and P. G. Petropoulos, "A staggered fourth-order accurate explicit finite difference scheme for the time-domain Maxwell's equations," *J. Comput. Phys.*, vol. 168, no. 2, pp. 286–315, Apr. 2001.

[16] S. Zhao and G. W. Wei, "High-order FDTD methods via derivative matching for Maxwell's equations with material interfaces," *J. Comput. Phys.*, vol. 200, no. 1, pp. 60–130, Oct. 2004.

[17] J.-P. Berenger, "A perfectly matched layer for the absorption of electromagnetic waves," *J. Comput. Phys.*, vol. 114, no. 2, pp. 185–200, Oct. 1994.

Theodoros T. Zygiridis, photograph and biography not available at time of publication.

Theodoros D. Tsiboukis (S'79–M'81–SM'99), photograph and biography not available at time of publication.